Modelling of intact and jointed mudstone samples under uniaxial and triaxial compression

Wai Loong Chong · Asadul Haque ·
Ranjith Pathegama Gamage · Akm Shahinuzzaman

Abstract Rock mass is a highly complex entity where the strength and deformation behaviour can be significantly affected by its secondary structures such as joints, fissures and bedding planes. Whilst many research works have been conducted to study the behaviour of a specific rock mass, a thorough understanding of its strength and deformation behaviour incorporating different joint sets has not been established. In this study, a comprehensive numerical modelling using a three-dimensional distinct element code, 3DEC, was undertaken to study the strength and deformation behaviour of a mudstone, locally found in Melbourne, in unconfined and confined states. The initial unconfined model established for intact mudstone was calibrated against the well-established laboratory-based empirical strength relationships and subsequently compared with some strength test data available for field samples. The intact unconfined model was then extended to study the strength behaviour in the confined state. The results obtained from this confined intact model were compared with existing strength criteria and were found in good agreement. The confined model was extended further to investigate the effects of joint sets and dip angles on the rock mass strength and deformation behaviour by incorporating two different joint configurations (one-joint and two-joint) with varying dip angles (0°–90°). This study found that the rock mass strength in a confined state varied significantly between the two joint configurations.

W. L. Chong · A. Haque (✉) · R. P. Gamage
Department of Civil Engineering, Monash University,
Clayton 3800 Victoria, Australia
e-mail: asadul.haque@monash.edu

A. Shahinuzzaman
Powerlink Queensland,
Harold Street,
Virginia 4014 Queensland, Australia

Introduction

The strength and the deformation behaviour of jointed rock mass have always been crucial in geotechnical engineering especially for designing foundations, tunnels and underground constructions. However, the determination of the strength of rock mass containing joints, fissures and bedding planes seems to be the most difficult aspect in rock mechanics. Many research works have been conducted to study the effects of these secondary structures on rock mass strength (Yang et al. 1998; Gong et al. 2006). Ramamurthy and Arora (1994) found that the number of joint, joint inclination and joint strength or roughness can affect the rock mass strength and deformation mechanism significantly. Many laboratory triaxial tests were carried out on different types of rocks such as slate (Donath 1972), shale (McLamore and Gray 1967) and granite (Ranjith et al. 2003) to determine the critical joint dip angle. In general, they found that the critical joint dip angle, where minimum strength occurs, follows the relationship proposed by Hoek and Brown (1980a, b), as shown in Fig. 1.

The study on rock mass strength in confined (triaxial) condition had also been carried out using numerical methods. Recently, Verma and Singh (2010) conducted numerical modelling using FLAC 3D to simulate triaxial tests on a rock containing a single fracture with different joint dip angles. The results obtained from the numerical study matched quite closely with the theoretical model, as shown in Fig. 2. However, they did not specify the rock type simulated as well as how the input properties were derived. As numerical modelling is very sensitive to the input properties of the material simulated, it is important to
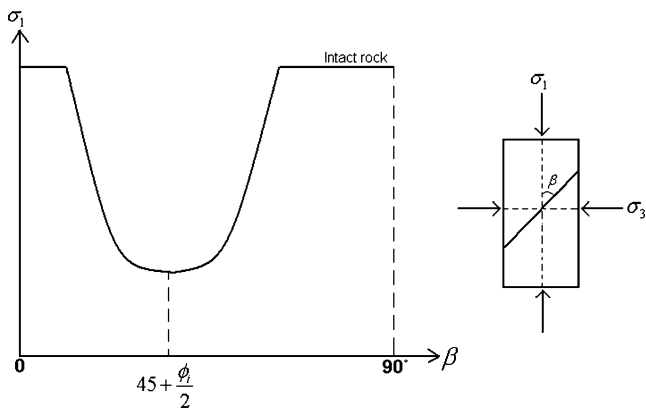
Fig. 1 Variation of peak strength with joint dip angle

ensure that the properties are representative of the actual material. The model used in their study was also not calibrated with laboratory or field test results.

So far, comprehensive numerical modelling of the strength and deformation behaviour of jointed rock mass under unconfined and confined states has not been conducted in great depth, especially for the local Melbourne mudstone. Whilst the properties of mudstone such as modulus and unconfined compressive strength (UCS) as a function of water content have been well established (Chiu 1981), the effect of physical joint sets with different dip angles on the strength and deformation behaviour of the rock has not been studied.

In this paper, a three-dimensional distinct element code, 3DEC (Itasca 2008), is employed to investigate numerically the effect of joint sets and dip angles on the strength and deformation behaviour of mudstone. The first section of the paper presents a brief background information of the Melbourne mudstone and the modelling of the unconfined state (UCS) for intact rock simulating the properties of the local mudstone. The simulated results compared well with the laboratory results of Johnstone rock (Johnston and Choi
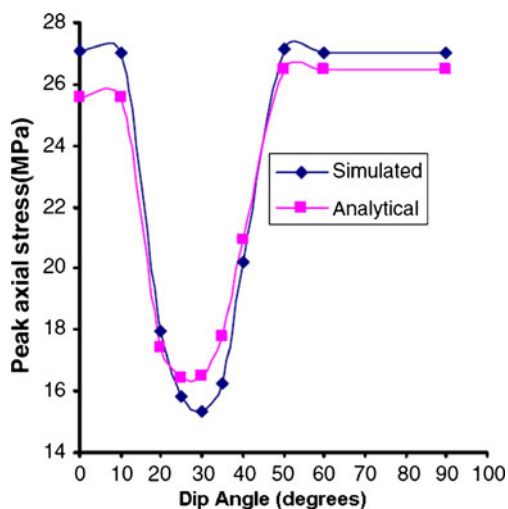

Fig. 2 Triaxial tests results simulated in FLAC 3D and theoretical prediction (Verma and Singh 2010)
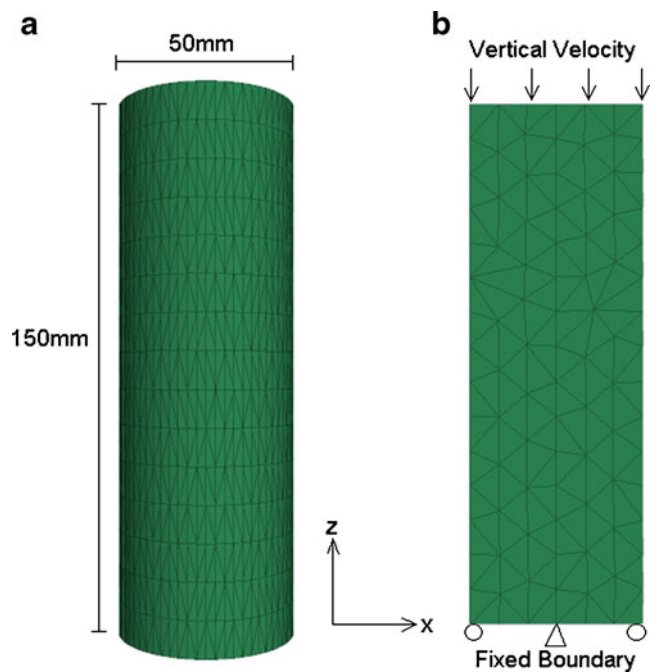

Fig. 3 a Three-dimensional illustration of the rock sample. b Cross-section of sample

1986) simulating the behaviour of Melbourne mudstone (Chiu 1981) and some natural mudstone samples. The model is then extended by applying confining stress around the intact mudstone model to simulate triaxial stress state. To calibrate the confined model for the intact mudstone, several methods (Mohr–Coulomb; Hoek and Brown 1980a, b; Johnston 1985) available in the literature for predicting the strength of the rock were used; the numerical results were found to be comparable with these methods. To study the effect of joint set and joint dip angle on the strength and deformation behaviour of mudstone in confined condition, two different jointing configurations (one-joint and two intersecting joints) with dip angles varying from 0° to 90° were subsequently simulated. The critical dip angle with the lowest peak axial stress was found to be 30° with vertical for the two joint configurations modelled. It was also observed that the rock mass strengths vary substantially between the two joint configurations simulated, which were explained with the help of the deformation mechanisms of the jointed mudstone.

Table 1 Input properties of mudstone rock

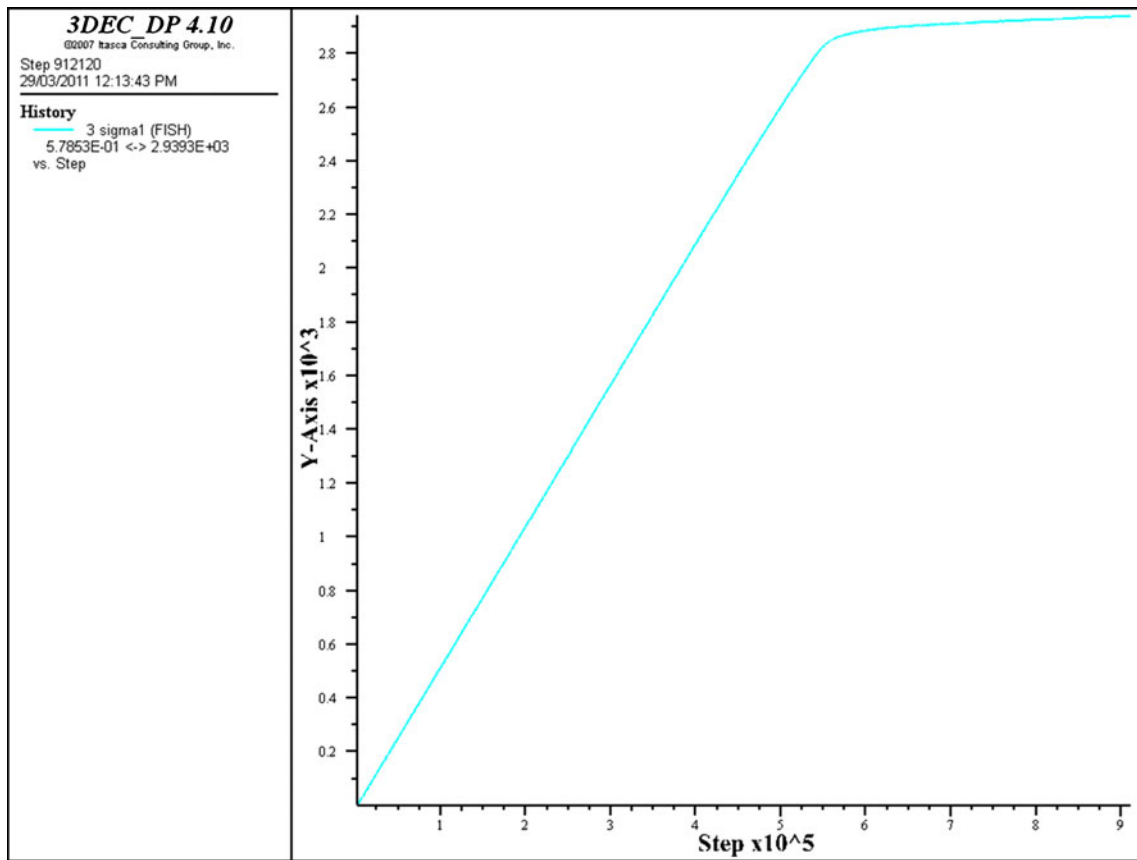| Water content, w (%)	10
Density, γ (kg/m^3)	2,300
Rock mass modulus, E (MPa)	538
Poisson's ratio, v	0.3
Friction angle, φ (deg)	38
Cohesion, c (kPa)	713
Tensile strength, σ_t (kPa)	355

Fig. 4 UCS plot for 10% water content intact mudstone model

Modelling of the unconfined strength behaviour of mudstone

The bedrock of Melbourne is a silurian formation which consists of interbedded mudstone, siltstone and sand-stone, and is more commonly known as the Melbourne Formation. The mudstone can be classified as a soft or weak rock as its mechanical strength is heavily affected by the degree of weathering of the material. Johnston (1992) found that the uniaxial compressive strength of a

Table 2 Mudstone properties for various water contents

Water content (%)	Poisson's ratio	Rock modulus (MPa)	Cohesion (kPa)	Friction angle	Tensile (kPa)
1	0.097	2,710	2,487	44	1,862
3	0.131	1,892	1,884	43	1,288
5.1	0.167	1,298	1,408	41	875
5.8	0.179	1,144	1,277	41	769
6.5	0.191	1,009	1,159	40	676
7.1	0.201	906	1,066	40	605
9.2	0.236	621	797	38	411
10.1	0.252	529	703	38	348
10.3	0.255	510	684	38	336
10.9	0.265	458	629	37	301
11.8	0.281	390	555	37	255
12.1	0.286	369	533	36	241
13.4	0.308	292	445	35	190

fresh, dark blue-coloured mudstone is around 10 MPa, whilst that of a highly weathered, yellow-coloured mudstone is as low as 1 MPa. In this paper, extensive numerical simulations of the strength and deformation behaviour of the mudstone were carried out using representative mudstone properties.

Model setup

An initial model of intact mudstone in the unconfined state was first simulated using 3DEC in order to calibrate the numerical model with laboratory test data available for Johnstone and natural mudstone samples. A cylindrical sample having a diameter of 50 mm with height of 150 mm was modelled as shown in Fig. 3. The centre node of the bottom of the sample was fixed in all directions to keep the sample in place, whilst the remaining nodes were restricted by not allowing movement in the z direction. The nodes at the side were prescribed roller boundary condition. A constant vertical compressive velocity of 0.1 mm/step was applied on top of the sample. A FISH subroutine (the built-in programming language in 3DEC) was written to convert the measured compressive velocity into force by reading the reaction of the nodes on top of the sample. The UCS of the rock can then be determined by dividing the peak force measured with the cross-sectional area of the sample. An elastic–perfectly plastic constitutive model and a Mohr–Coulomb type of failure were assigned to the rock. The input properties, based on well-established empirical relationships for mudstone (Chiu 1981), for a typical water content of 10% are shown in Table 1. Figure 4 shows a typical applied stress plot in 3DEC depicting the peak stress at failure of 2.85 MPa.

Unconfined compressive strength

Different water contents of mudstone ranging from 1% to 14% were simulated in 3DEC. The mudstone properties for input to 3DEC were calculated using empirical relationships derived by Chiu (1981), as shown in Table 2. The UCS corresponding to the mudstone water contents were also computed using Chiu (1981). Figure 5 shows the UCS results obtained from 3DEC together with the laboratory results of Johnstone and field samples. It can be seen that the 3DEC estimations of UCS for the different water contents simulated match closely with the laboratory results of synthetic mudstone (Johnstone). The numerical predictions also provided a reasonable comparison with the natural mudstone (R^2=0.77). This indicates the suitability of using numerical package such as 3DEC to reliably predict the strength of mudstone rock under unconfined condition.
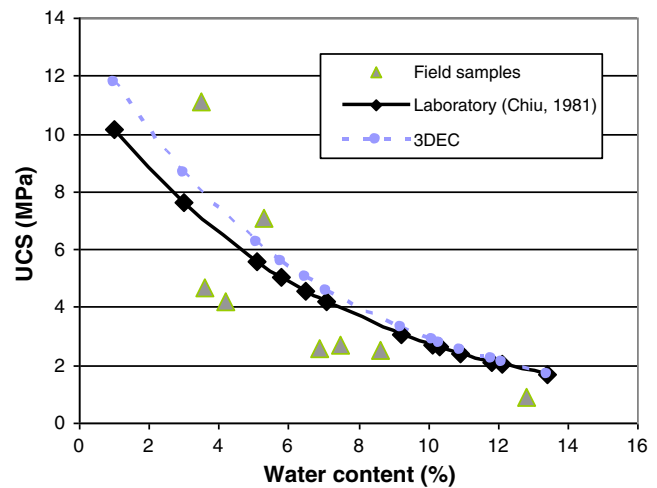

Fig. 5 Variation of UCS with water content

Modelling of the confined strength behaviour of mudstone

Intact rock model

The mudstone model under the unconfined state presented previously was employed to simulate the confined condition (triaxial) by applying confining pressure to the periphery of the sample. A constant compressive velocity was subsequently applied on top of the sample. Intact rock condition was first simulated and the peak stress recorded for each confined stress condition. The observed peak stresses at various confining stresses were then compared with several methods (Mohr–Coulomb; Hoek and Brown 1980a, b; Johnston 1985) to calibrate the 3DEC model. The peak axial stress for a rock with UCS of 1 MPa obtained from the numerical model under a confining pressure of 50 kPa was 1,155 kPa. The three available methods, as shown respectively in Eqs. 1–3, gave peak strength estimations of 1,150, 1,254 and 1,204 kPa, respectively. The predicted values are in good agreement with the 3DEC output. With this, the model was subsequently extended to investigate the effect of joint sets (one-joint and two-joint) and dip angles on the strength of mudstone under the confined condition.

Mohr–Coulomb:

$$\sigma_1 = \sigma_c + \sigma_3 \left(\frac{1 + \sin \varphi}{1 - \sin \varphi} \right) \tag{1}$$

where σ_c is the UCS of rock

Hoek and Brown (1980a, b):

$$\sigma_1 = \sigma_3 + \sigma_c \left(m \frac{\sigma_3}{\sigma_c} + 1 \right) \tag{2}$$
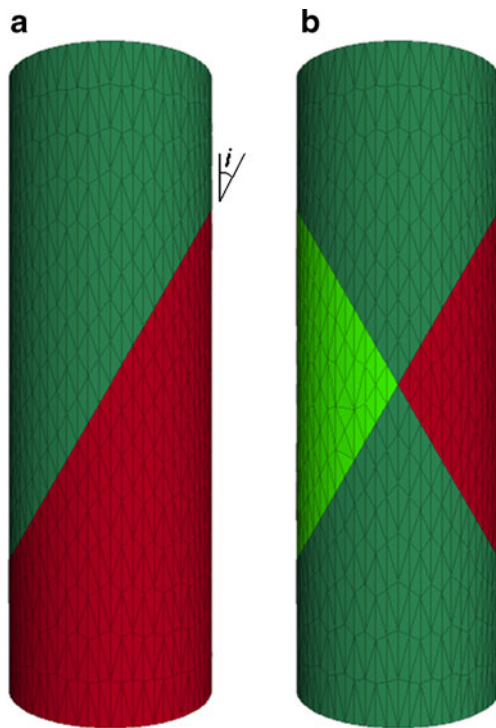
Fig. 6 One-joint (a) and two-joint (b) models

where $m=9$ for siltstone

Johnston ([1985]):

$$\sigma_1 = \sigma_c \left(\frac{m}{B} \frac{\sigma_3}{\sigma_c} + 1 \right)^B \qquad (3)$$

where:

$B = 1 - 0.0172 \log \sigma_c^2$
$m = 2.065 - 0.231 \log \sigma_c^2$

Mudstone with one joint in the confined state

The calibrated intact mudstone model was extended to study the effect of joint sets (one-joint and two-joint)
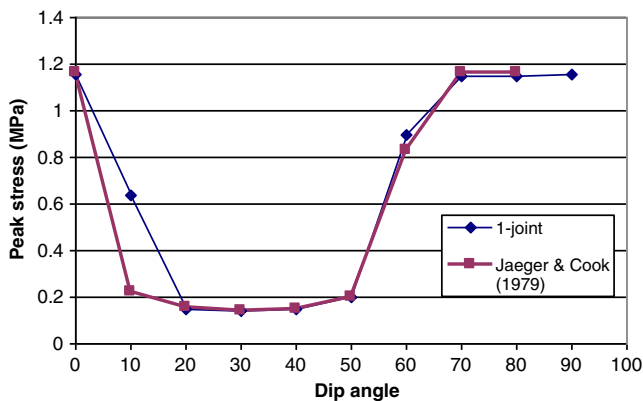

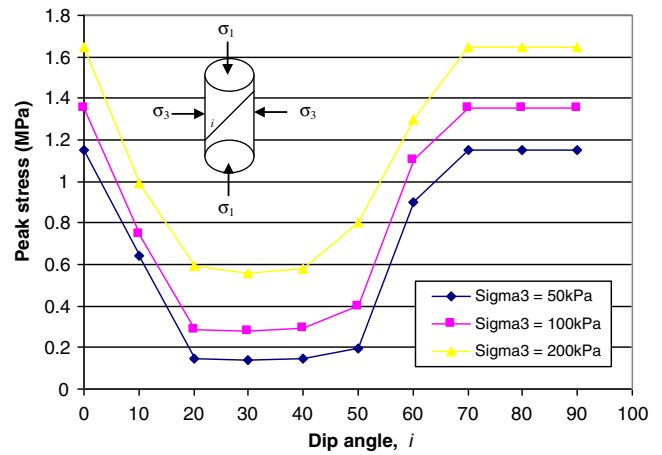Fig. 7 Comparison between 3DEC results and analytical predictions

Fig. 8 Comparison of peak stresses with different confining pressures for the one-joint model

and dip angles (0°–90°) on the strength and deformation mechanisms of the jointed mudstone. Two different joint configurations were simulated, as illustrated in Fig. 6. A typical friction angle representing a jointed mudstone of 28° was assigned to the joint in the numerical model. A Mohr–Coulomb slip constitutive model was prescribed to govern the joint deformation behaviour.

The one-joint mudstone model shown in Fig. 6a was simulated in the confined condition using a confining pressure of 50 kPa for joint dip angles of 0–90° with an interval of 10°. Figure 7 shows the peak axial stresses obtained for the dip angles modelled together with the values obtained from the analytical method of Jaeger and Cook ([1979]), as shown in Eq. 4. It was found that the dip angle of 30° with vertical resulted in the lowest peak axial stress, which is in agreement with the theoretical critical joint dip angle of $45 - \phi/2$ as well as with Jaeger and Cook ([1979]). With this, two higher confining stresses of 100 and
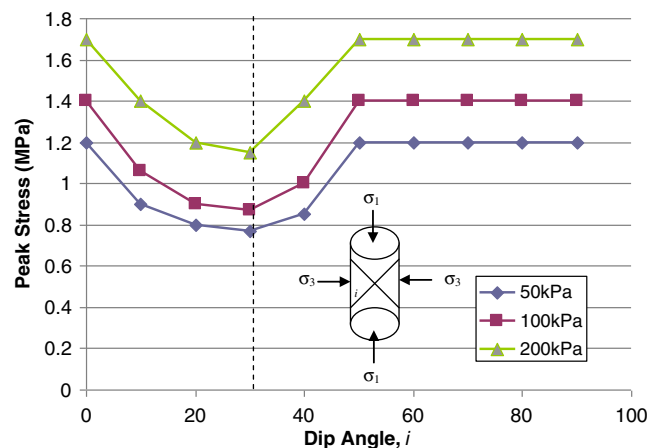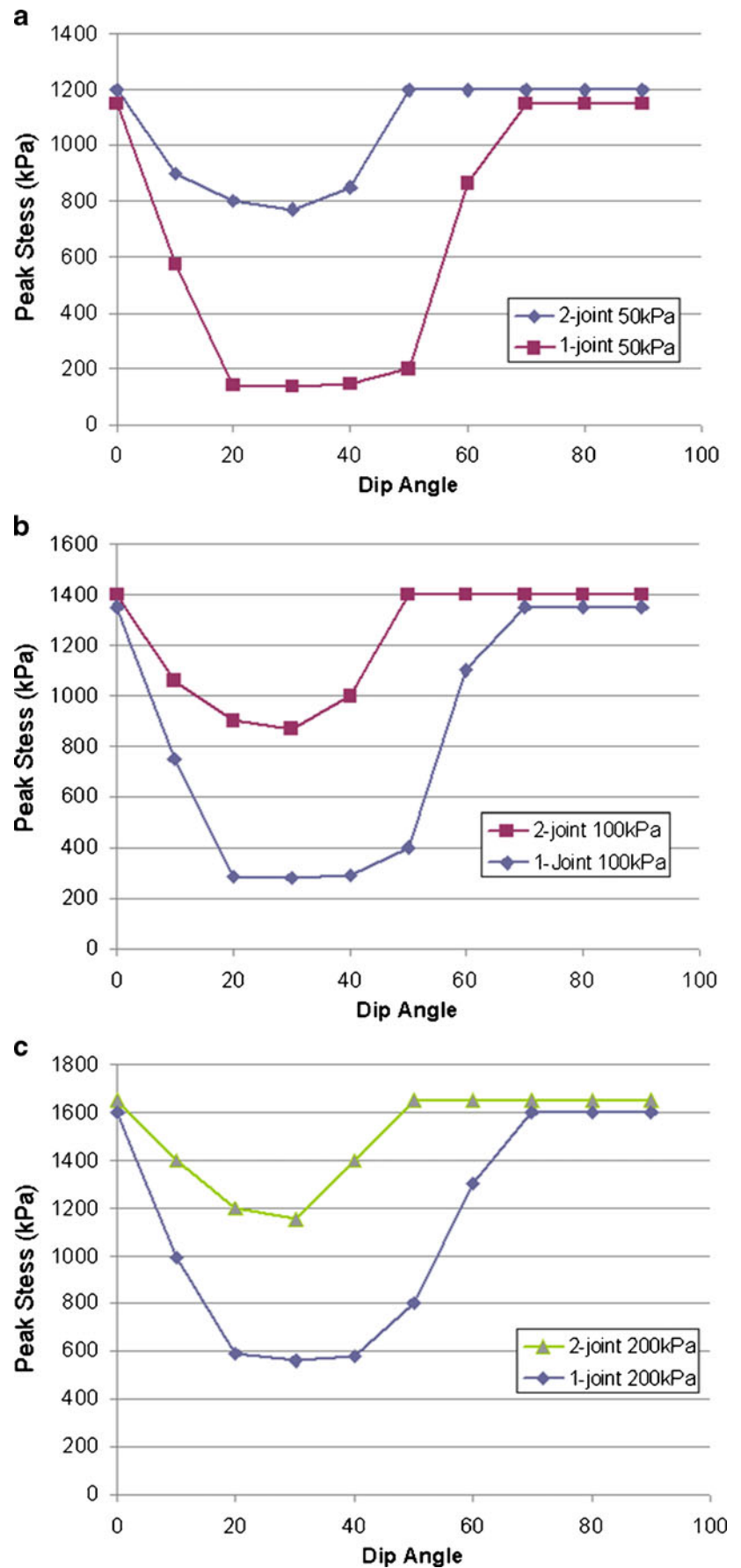

Fig. 9 Comparison of peak stresses with different confining pressures for the two-joint model

Fig. 10 Comparison of peak strengths between the one-joint and two-joint models for different confining stresses

200 kPa were subsequently investigated; the comparison between different confining stresses is shown in Fig. 8. It is not surprising that an increase in confining stress increases the peak axial stress of the jointed rock samples. It can also be observed that the critical joint dip angle of 30° remained unchanged with higher confining pressures.

$$\sigma_1 = \sigma_3 + \frac{2(S_w + \tan \phi_w \sigma_3)}{(1 - \tan \phi_w \cot \beta) \sin 2\beta} \qquad (4)$$

where S_w is the shear strength of joint, ϕ_w is the friction angle of joint and β is the joint inclination from vertical axis.

Mudstone with two joints in the confined state

The effect of a single joint in the simulated mudstone rock under the confined condition has been shown to give a critical dip angle of 30° where the minimal peak strength occurred. In this subsequent investigation, another joint set was incorporated for the confined state, as shown in Fig. 6b. The 3DEC numerical modelling was conducted for the same confining stresses of 50, 100 and 200 kPa. Figure 9 presents the results of peak axial stresses for joint dip angles varying from 0° to 90°. It is not surprising that as the confining pressure increases, the strength of the simulated mudstone with two-joint set also increases. It can be seen that the critical joint dip angle for the two-joint set condition depicts the same angle of 30°.

Effect of joints on the deformation behaviour of jointed rock in the confined state

The results obtained for one-joint and two-joint models showed a critical joint dip angle of 30° for both the cases, where the peak strength was at its lowest compared with other dip angles. However, it was observed that the peak stress and failure mechanisms of both joint conditions have marked differences. Figure 10 depicts the comparisons of the peak stresses for different joint dip angles at the three confining pressures simulated for the one-joint and two-joint models. It can be seen that the two-joint condition demonstrates almost three times the strength of the one-joint model for a given joint dip angle of 30°. This is surprising due to the fact that a more jointed rock should exhibit lower strength. The explanation of this finding was found by examining the failure mechanisms of the jointed mudstone in the confined state. Figure 11 presents the 3DEC plasticity plots for the one-joint and two-joint models for the critical joint dip angle of 30°, where the non-blue colour denotes shear/tensile failures of the mudstone.

As shown in Fig. 11, the extent of rock failure in both the models varies significantly. For the one-joint case
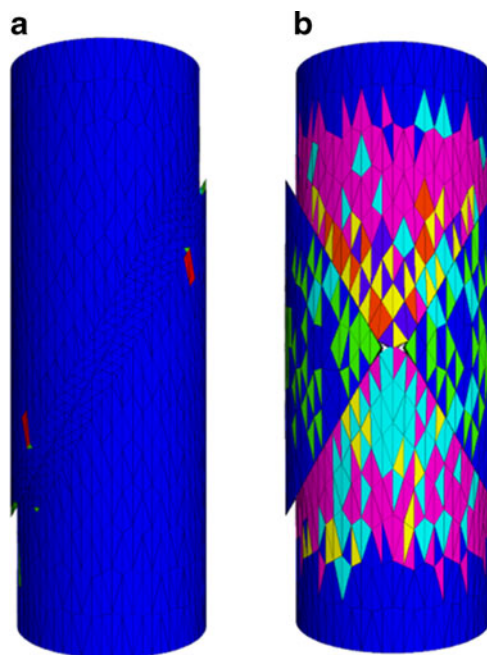

Fig. 11 Failure plots for the one-joint model (a) and the two-joint model (b)

(Fig. 11a), very minimal intact rock failure is observed, which implies that the strength of the rock is governed by the frictional sliding along the weakness plane. This is contrary to the two-joint case, as depicted in Fig. 11b. Extensive rock failures can be observed due to the compression of the top and bottom major rock blocks when the two minor side blocks are sliding outwards. The development of the shear and tensile failures at different stages for the two-joint model is illustrated in greater detail in Fig. 12.
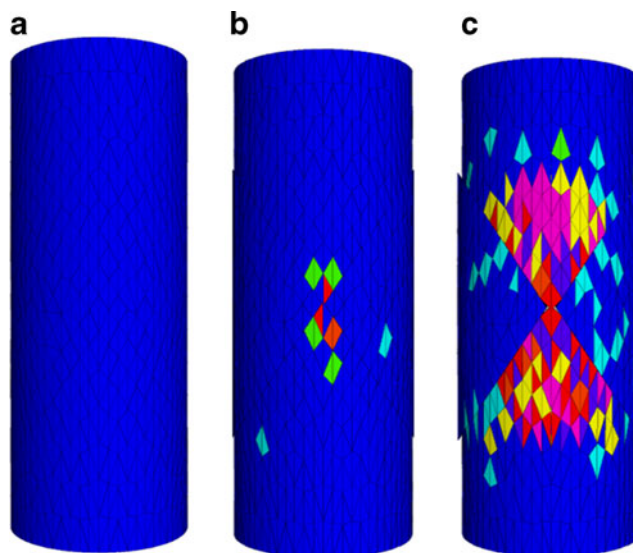

Fig. 12 a Initial condition. After vertical displacement of 1.5 mm (b) and 5 mm (c)

Figure 12a depicts the initial condition before the compression force is applied on the mudstone. At 1.5 mm of compression displacement (Fig. 12b), the rock material at the position where both joints intersect starts to develop shear failure. This is due to the intersection of the two joints forming two rock tips that compress against each other, resulting in intact rock failure. At further compression displacement of 5 mm (Fig. 12c), more extensive rock failure can be observed. The higher strength obtained in the two-joint model compared with the one-joint model can be explained by the mobilisation of intact rock strength during the rock deformation. For the one-joint case, intact rock failure is almost negligible as failure is dominated by the joint slip, as shown in Fig. 11a.

Conclusion

Rock mass is a highly complex entity where the strength and deformation behaviour can be significantly affected by its secondary structures such as joints, fissures and bedding planes. Although many research works have been conducted in this area, a thorough understanding of the strength and deformation behaviour of rock mass incorporating various joint sets and orientations has not been well established especially for Melbourne mudstone. In this study, a comprehensive numerical modelling has been carried out to simulate the strength and deformation behaviour of intact and jointed mudstone under the confined and unconfined states.

In the numerical simulation of mudstone in the unconfined state, very good agreement was achieved when the UCS values obtained from numerical modelling were compared with the results of synthetic and natural mudstone. Under the confined condition, the peak stress for intact mudstone was found to match the empirical results closely. The calibrated model was subsequently extended to incorporate one and two joints with dip angles varying between 0° and 90°. It was observed that the corresponding peak stress for the one-joint condition closely matched an analytical method available in the literature. The critical dip angle with the lowest peak stress for the one-joint case was 30° with vertical, which is consistent with the theoretical critical joint dip angle of $45 - \phi/2$.

For the two-joint condition, the critical angle obtained was identical with the one-joint case (30°). However, it was observed that the strength of mudstone with different simulated dip angles was markedly higher than the one-joint model. This was due to the considerable mobilisation of the intact rock strength for the two-joint model where shear and tensile failures were observed. The two intersecting joints formed two rock tips that compressed against each other and hence resulted in the intact rock failure. However, for the one-joint condition, the strength was mainly derived from frictional sliding along the joint plane.

References

Chiu HK (1981) Geotechnical properties and numerical analysis for pile design in weak rock. PhD thesis, Department of Civil Engineering, Monash University

Donath FA (1972) Effects of cohesion and granularity on deformation behaviour of anisotropic rock. In: Doe BR, Smith DK (eds) Studies in mineralogy and Precambrian geology. Geological Society of America Memoir, 135, pp 95–128

Gong QM, Jiao YY, Zhao J (2006) Numerical modelling of the effects of joint spacing on rock fragmentation by TBM cutters. Tunn Undergr Space Technol 21:46–55

Hoek E, Brown ET (1980a) Underground excavations in rock. E & FN Spon, London

Hoek E, Brown ET (1980b) Empirical strength criterion for rock masses. J Geotech Eng ASCE 106:1013–1035

Itasca (2008) 3DEC user's guide. Itasca Consulting Group Inc., Minnesota

Jaeger JC, Cook NGW (1979) Fundamentals of rock mechanics, 3rd edn. Chapman and Hall, London, pp 134–144

Johnston IW (1985) Strength of intact geomechanical materials. J Geotech Eng ASCE 111:739–749

Johnston IW (1992) Silurian and lower Devonian engineering properties. In: Peck, Nielson, Olds, Seddon (eds) Engineering geology of Melbourne. Balkema, Rotterdam 95–108

Johnston IW, Choi SK (1986) A synthetis soft rock for laboratory model studies. Geotechnique 35(2):251–263

McLamore R, Gray KE (1967) The mechanical behaviour of anisotropic sedimentary rocks. J Eng Industry Trans A Soc Mech Eng Ser B 89:62–73

Ramamurthy T, Arora VK (1994) Strength predictions for jointed rocks in confined and unconfined states. Int J Rock Mech Min Sci 31(1):9–22

Ranjith PR, Siew FP, Hefny AM, Zhao J (2003) Strengths and mechanics of fractured rocks under triaxial loadings. ISRM 2003—Tech Roadmap Rock Mech, South African Institute of Mining and Metallurgy

Verma AK, Singh TN (2010) Modelling of a jointed rock mass under triaxial conditions. Arab J Geosci 3:91–103

Yang ZY, Chen JM, Huang TH (1998) Effect of joint sets on the strength and deformation of rock mass models. Int J Rock Mech Min Sci 35:75–84